Monthly Notices
of the
ROYAL ASTRONOMICAL SOCIETY

MNRAS **502,** L99–L103 (2021)
Advance Access publication 2021 January 29

doi:10.1093/mnrasl/slab008

Massive black hole binary systems and the NANOGrav 12.5 yr results

H. Middleton [1,2★] A. Sesana,[3,4★] S. Chen,[5,6★] A. Vecchio,[7] W. Del Pozzo [8,9] and P. A. Rosado[10]

[1]*School of Physics, University of Melbourne, Parkville, VIC 3010, Australia*
[2]*OzGrav-Melbourne, ARC Centre of Excellence for Gravitational-Wave Discovery, University of Melbourne, VIC 3010, Australia*
[3]*Department of Physics 'G. Occhialini', University of Milano–Bicocca, Piazza della Scienza 3, I-20126 Milano, Italy*
[4]*INFN Sezione di Milano–Bicocca, Piazza della Scienza 3, I-20126 Milano, Italy*
[5]*Laboratoire de Physique et Chimie de l'Environnement et de l'Espace, Université d'Orléans, CNRS, F-45071 Orléans, France*
[6]*Station de Radioastronomie de Nançay, Observatoire de Paris, PSL University, CNRS, F-18330 Nançay, France*
[7]*School of Physics and Astronomy & Institute for Gravitational Wave Astronomy, University of Birmingham, Birmingham B15 2TT, UK*
[8]*Dipartimento di Fisica 'Enrico Fermi', Universit di Pisa, I-56127 Pisa, Italy*
[9]*INFN Sezione di Pisa, I-56127 Pisa , Italy*
[10]*Holaluz-Clidom S.A., Passeig de Joan de Borb 99-101, 4a Planta, E-08039 Barcelona, Spain*

Accepted 2021 January 20. Received 2021 January 7; in original form 2020 November 30

ABSTRACT

The North American Nanohertz Observatory for Gravitational Waves (NANOGrav) recently reported evidence for the presence of a common stochastic signal across their array of pulsars. The origin of this signal is still unclear. One possibility is that it is due to a stochastic gravitational-wave background (SGWB) in the ∼1–10 nHz frequency region. Taking the NANOGrav observational result at face value, we show that this signal would be fully consistent with an SGWB produced by an unresolved population of in-spiralling massive black hole binaries (MBHBs) predicted by current theoretical models. Considering an astrophysically agnostic model, the MBHB merger rate is loosely constrained. Including additional constraints from galaxy pairing fraction and MBH–bulge scaling relations, we find that the MBHB merger rate is 1.2×10^{-5}-−$4.5 \times 10^{-4}\,\mathrm{Mpc^{-3}\,Gyr^{-1}}$, the MBHB merger time-scale is $\leq 2.7\,\mathrm{Gyr}$, and the norm of the $M_{\rm BH}-M_{\rm bulge}$ relation is $\geq 1.2 \times 10^{8}\,\mathrm{M_{\odot}}$ (all quoted at 90 per cent credible intervals). Regardless of the astrophysical details of MBHB assembly, the NANOGrav result would imply that a sufficiently large population of massive black holes pair up, form binaries and merge within a Hubble time.

Key words: black hole physics – gravitational waves – methods: data analysis; pulsars: general – galaxies: evolution – galaxies: formation.

1 INTRODUCTION

Accurate, decade-long timing of an ensemble of millisecond pulsars – a pulsar timing array (PTA) – provides a means to detect gravitational waves (GWs) in the nanohertz frequency band (Sazhin 1978; Detweiler 1979; Foster & Backer 1990). Over the last 20 yr, several PTAs have been used to achieve ever increasing sensitivity. One possible signal that could emerge from such timing campaigns is an isotropic, Gaussian stochastic gravitational-wave background (SGWB). As PTAs' peak sensitivity is sufficiently a narrow band, in this frequency range, the SGWB characteristic GW strain amplitude can be simply cast in the form

$$h_{\rm c}(f) = A_{\rm yr}\left(\frac{f}{1\,\mathrm{yr^{-1}}}\right)^{\alpha}, \tag{1}$$

where f is the GW frequency, $A_{\rm yr}$ is its (unknown) amplitude at the reference frequency of $1\,\mathrm{yr^{-1}}$, and α is the (unknown) spectral slope, which is related to the timing residuals' power spectral density, γ, by the relation $\gamma = 3 - 2\alpha$.

To date, several upper limits on the SGWB have been placed by PTA groups. The most stringent upper limit is from the Parkes PTA (PPTA; Shannon et al. 2015), $A_{\rm yr} \leq 1 \times 10^{-15}$ with 95 per cent confidence. The European PTA (EPTA; Lentati et al. 2015), North American Nanohertz Observatory for Gravitational Waves (NANOGrav; Arzoumanian et al. 2018), and the International PTA (IPTA; Verbiest et al. 2016) have also reported comparable upper limits, just a factor of ≈2 higher. However, NANOGrav have recently reported evidence for a common stochastic red process with an amplitude of 1.37–2.67×10^{-15} (5 per cent to 95 per cent quantiles) across 45 pulsars timed in their 12.5 yr data set (Arzoumanian et al. 2020), but with insufficient evidence for a Hellings and Downs correlation (Hellings & Downs 1983). The odds of a common versus independent signal are ∼10^3–10^4:1, depending on the assumptions in the analyses. This detection is in tension with previously published upper limits by NANOGrav (Arzoumanian et al. 2018) and, more noticeably, PPTA (Shannon et al. 2015), but Arzoumanian et al. (2020) and Hazboun et al. (2020) suggest that problems with the ephemeris and noise model in previous analyses may have conspired to underestimate previously reported upper-limit values.

Taking the NANOGrav result at face value, several authors have recently argued that a number of processes such as first-order phase transitions, cosmic strings, domain walls, large amplitude curvature

★ E-mail: hannah.middleton@unimelb.edu.au(HM);
alberto.sesana@unimib.it (AS); siyuan.chen@cnrs-orleans.fr(SC)

perturbations, and primordial black holes' inflation can indeed produce an SGWB with amplitude and spectral index consistent with this result. However, over the years, one of the main drivers for pursuing PTAs as GW detectors has been the astrophysical scenario of an SGWB produced by the incoherent superposition of gravitational radiation from adiabatically in-spiraling massive black hole binaries (MBHBs) at the centre of galaxies. Individual massive black holes (MBHs) exist at the centres of most galaxies (Kormendy & Ho 2013), and hierarchical galaxy formation scenarios indicate that galaxy mergers are frequent throughout cosmic time (White & Rees 1978; Begelman, Blandford & Rees 1980).

We show that this scenario is fully consistent with the NANOGrav results, which would further provide some initial mild constraints on crucial parameters of MBHB assembly models. In Section 2, we consider Monte Carlo realizations of the SGWB from Rosado, Sesana & Gair (2015) to demonstrate the consistency of the expected spectral properties of this signal with the constraints placed by the NANOGrav analysis. In Section 3, we describe our use of Bayesian inference with parametric models of the SGWB signal. The models are based on two sets of assumptions for the underlying MBHB population: an agnostic phenomenological population model in which binaries are assumed in circular orbits and on which we impose minimal prior constraints following Middleton et al. (2016); and an astrophysically driven model which accounts for binary eccentricity as in Chen, Sesana & Del Pozzo (2017b), Chen et al. (2017a), and Middleton et al. (2018), and includes coupling with the environment and additional constraints from independent observations regarding galaxy pair fraction, and $M_{\rm BH}$–$M_{\rm bulge}$ relation following Chen, Sesana & Conselice (2019). We present our results in Section 4 and our main findings are summarized in Section 5.

2 GRAVITATIONAL-WAVE SIGNAL FROM MBHBS

We start by showing that the results reported by NANOGrav are consistent with existing theoretical predictions of assembly and evolution of MBHBs. This is necessary because the NANOGrav posterior of the inferred spectral index is centred at $\gamma > 13/3$, a feature prompting a number of interpretations related to an early Universe origin, which would produce steeper red spectra compared to a population of MBHBs.

Assuming that MBHBs have circular, GW-driven orbits, the characteristic strain of the SGWB, equation (1), can be computed by integrating over the population distribution in redshift, z, and chirp mass, $\mathcal{M}$, where $\mathcal{M}$ is a combination of the binary component masses m_1 and m_2 given by $\mathcal{M} = (m_1 m_2)^{3/5}(m_1 + m_2)^{-1/5}$, according to Phinney (2001)

$$h_{\rm c}^2(f) = \frac{4G^{5/3}}{3\pi^{1/3}c^2} f^{-4/3} \int {\rm d}\mathcal{M} \int {\rm d}z (1+z)^{-1/3} \mathcal{M}^{5/3} \frac{{\rm d}^2 n}{{\rm d}z{\rm d}\mathcal{M}}, \quad (2)$$

where G and c are the gravitational constant and speed of light, respectively. The population of sources is described by the distribution ${\rm d}^2n/({\rm d}z{\rm d}\mathcal{M})$ as the number density of binaries per unit redshift and chirp mass interval.

Equation (2) expresses the SGWB in terms of its average energy density as a function of frequency, and results by construction in a continuous, smooth spectrum. In reality, the signal is given by an incoherent superposition of discrete quasi-monochromatic sources that can significantly depart from isotropy, Gaussianity, and even result in individually resolvable systems (Sesana, Vecchio & Volonteri 2009; Cornish & Sesana 2013; Taylor, van Haasteren & Sesana 2020). Crucially, since the signal is dominated by the loudest

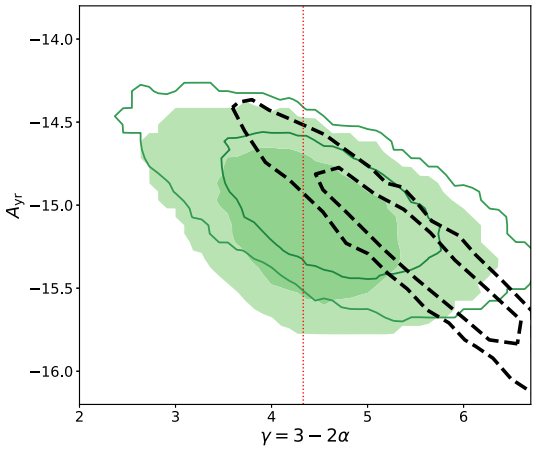

Figure 1. 68 per cent and 95 per cent credible regions of the amplitude and slope ($A_{\rm yr}$, γ) of the common red signal detected by NANOGrav (black contours) and predicted by the Monte Carlo MBHB population from Rosado et al. (2015) (green contours). Filled contours are for the complete suite of 234 K models while open contours are only for models featuring the revised MBH–host relations (see the main text for details). The dashed vertical line indicates $\gamma = 13/3$.

sources, the local spectral shape can significantly depart from the average slope defined by equation (2). To test this statement we proceed as follows. The SGWB spectrum is resolved in bins $\Delta f_i = 1/T$, where T is the baseline of the observing PTA. A practical way to compute the actual signal spectrum is as follows: convert ${\rm d}^2n/({\rm d}z{\rm d}\mathcal{M})$ into a ${\rm d}^3N/({\rm d}z{\rm d}\mathcal{M}{\rm d}f)$ – i.e. the distribution of sources emitting per unit chirp mass, redshift, and frequency – make a Monte Carlo draw from this distribution, and add up the signal from each individual binary to obtain

$$h_{\rm c}^2(f_i) = \frac{\sum_k h_k^2 f_k}{\Delta f_i}. \quad (3)$$

Here Δf_i is the ith frequency bin over which the GW spectrum is resolved; the sum runs over all the k sources emitting in the ith frequency bin; and h_k is the inclination–polarization averaged strain emitted by each individual MBHB in the Monte Carlo drawing (see Sesana, Vecchio & Colacino 2008, for details).

We compute the SGWB characteristic amplitude $h_{\rm c}(f)$ from the 234 K Monte Carlo MBHB populations presented in Rosado et al. (2015). For each realization of the population, we compute the predicted SGWB strain according to equation (3), using the same binning of the NANOGrav 12.5-yr power spectrum (i.e. $\Delta f_i = f_{i+1} - f_i$, where $f_i = i/(12.5{\rm yr})$). We then make a least-square fit to a single power law for $h_{\rm c}$ and construct 234 K pairs of coefficients ($A_{\rm yr}$, γ). Fig. 1 compares probability density contours of ($A_{\rm yr}$, γ) obtained with this procedure to that inferred from NANOGrav data. Although centred around $\gamma = 13/3$, the 95 per cent credible theoretical region extends in the range $3 \lesssim \gamma \lesssim 6$, and there is a significant overlap in the 2D 68 per cent credible region predicted by the models and measured by NANOGrav. The models were constructed employing a large set of MBH–host relations published in the literature over two decades. In particular, the discovery of overmassive black holes in bright cluster ellipticals, together with the amendment of several dynamical individual MBH mass measurements, prompted an upward revision of the MBH–bulge relations (Graham 2012; Kormendy & Ho 2013; McConnell & Ma 2013). If we limit our set to those models, the expected ($A_{\rm yr}$, γ) contours shift to the upper right, showing an even higher level of consistency with the published NANOGrav posterior.

3 SGWB MODELLING AND ASTROPHYSICAL INFERENCE METHOD

Now we have established consistency of the NANOGrav result with theoretical predictions about MBHB populations; we consider parametric models describing this population and employ Bayesian inference to explore implications and constraints on the underlying astrophysical model parameters. For this study, we consider two specific population models.

The first model was developed by Middleton et al. (2016, M16 hereinafter). Binaries are assumed to have circular GW-driven orbits. The SGWB characteristic amplitude is fully described by equation (2), and we make only minimal assumptions about the MBHB population. We model $\mathrm{d}^2n/(\mathrm{d}z\mathrm{d}\mathcal{M})$ as a Schechter function (Schechter 1976) of the form

$$\frac{\mathrm{d}^2n}{\mathrm{d}z\,\mathrm{d}\log_{10}\mathcal{M}} = \dot{n}_0\left[\left(\frac{\mathcal{M}}{10^7\mathrm{M}_\odot}\right)^{-\alpha_\mathcal{M}}\exp^{-\mathcal{M}/\mathcal{M}_*}\right] \times\left[(1+z)^{\beta_z}\exp^{-z/z_0}\right]\frac{\mathrm{d}t_\mathrm{R}}{\mathrm{d}z}\,, \quad (4)$$

where t_R is the time in the source rest frame and we assume cosmological parameter values of $H_0 = 70\,\mathrm{km\,s^{-1}\,Mpc^{-1}}$ (i.e. $h_0 = 0.7$), $\Omega_M = 0.3$, $\Omega_\Lambda = 0.7$, and $\Omega_k = 0$. The shape and magnitude of the population distribution are described by five parameters: $\theta = \{\dot{n}_0, \alpha_\mathcal{M}, \mathcal{M}_*, \beta_z, z_0\}$, where $\{\alpha_\mathcal{M}, \mathcal{M}_*\}$ and $\{\beta_z, z_0\}$ control the shape of the $\mathcal{M}$ and z distributions, respectively, and $\dot{n}_0$ is the merger rate per unit rest-frame time, co-moving volume, and logarithmic $\mathcal{M}$ interval. The integration limits in equation (2) are set to $0 \le z \le 5$ and $10^6 \le \mathcal{M}/M_\odot \le 10^{11}$.

The second model follows Chen et al. (2019, C19 hereinafter). In this model, the MBHB population is allowed to include eccentric binaries and to interact with the environment, which can cause a departure of the SGWB characteristic amplitude $h_\mathrm{c}(f)$ from the single power-law behaviour described by equation (2). In this model, $h_\mathrm{c}(f)$ is described by 18 independent parameters related to the galaxy stellar mass function (described by a redshift evolving single Schechter function), the black hole pair fraction, merger time-scale, and galaxy–MBH scaling relation. We refer the reader to Chen et al. (2019) for full details. In summary, the MBHB merger rate $\mathrm{d}^2n/(\mathrm{d}z\mathrm{d}\mathcal{M})$ is described by 16 parameters related to astrophysical observables: (Φ_0, Φ_I, M_0, α_0, α_I) for the galaxy stellar mass function, (f_0', α_f, β_f, γ_f) for the pair fraction, (τ_0, α_τ, β_τ, γ_τ) for the merger time-scale, and (M_*, α_*, ϵ) for the M_BH–M_bulge scaling relation. The first three sets of parameters can be combined into five effective parameters that allow us to write the merger rate in the form given by equation (4), to ease comparison with the agnostic M16 model. Finally, two extra parameters, ζ_0 and e_0, describe the density of the stellar environment and the eccentricity at the MBHB pairing, respectively, and can produce a low-frequency departure of the spectrum from the single power-law of equation (2).

We use Bayesian inference to derive constraints on the underlying astrophysical model parameters from the observational data d. The joint posterior distribution $p(\theta|d, M)$ for the parameters θ of model M given d is

$$p(\theta|d, M) = p(\theta|M)p(d|\theta, M)/p(d|M)\,, \quad (5)$$

where $p(\theta|M)$ is the prior distribution on the model parameters, $p(d|\theta, M)$ is the likelihood of model M with parameters θ of producing the data, and $p(d|M)$ is the evidence.

We now specify the likelihood function $p(d|\theta, M)$ used in our analysis. The data d would naturally be the Monte Carlo Markov chains of the detected signal amplitudes at each frequency, f, derived by the NANOGrav analysis of the 12.5 yr data set (Arzoumanian et al. 2020). The chains have not been publicly released, so we construct analytical approximations for the posterior distribution of the detected signal. The M16 model takes, as a single data input, the measured signal amplitude at $f = 1\ \mathrm{yr}^{-1}$. We model it as a lognormal distribution centred around $\log_{10}A_\mathrm{yr} = -14.7$ with $\sigma = 0.09$, which reproduces the 5–95 per cent credible range in A_yr of $(1.37–2.67) \times 10^{-15}$ quoted by NANOGrav. For the C19 model, we take the same reference value and construct $d(f)$ (using an $\alpha = -2/3$ power law) of the five lowest frequency bins $f_i = i/T$ used in the 'free spectrum' analysis reported by NANOGrav, and assign an uncertainty of $\sigma_i = 0.09$ at each f bin. Thus, the likelihood function takes the general form

$$\log_{10} p\,(d|\theta, M) \propto -\frac{1}{2}\sum_f \frac{\left[\log_{10} A(f;\theta,\ M) - \log_{10} d(f)\right]^2}{\sigma^2(f)}\,, \quad (6)$$

where each frequency bin can be treated independently with its own detected strain amplitude $d(f)$ and uncertainty $\sigma(f)$. The predicted amplitude $A(f;\theta,\ M)$ from a given model M and parameter θ is then compared against the NANOGrav-detected amplitudes from the data $d(f)$, approximated following the procedure described earlier.

Next we specify the priors. The M16 priors are identical to those used in Middleton et al. (2016), with the exception of $\mathcal{M}_*$, which is now uniform in $\log_{10}\mathcal{M}_* \in [6, 10]$, and $\dot{n}_0$, which is now uniform in $\log_{10}\dot{n}_0 \in [-20, 3]$. For C19 we use the 'extended' prior range reported in table 1 of Chen et al. (2019). This choice of C19 priors produces a predicted range of the SGWB that is consistent with the Monte Carlo models of Rosado et al. (2015) considered in Section 2.

The joint posterior density distributions on the model parameters $p(\theta|d, M)$ (equation 5) are computed using `cpnest`, a nested sampler (Veitch & Vecchio 2010; Veitch et al. 2021) and `PTMCMCSampler`, a Markov-chain Monte Carlo-based sampler (Ellis & van Haasteren 2017).

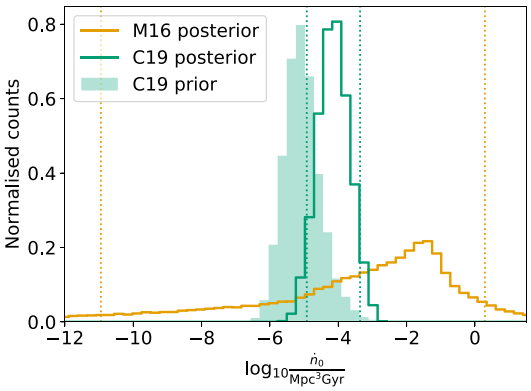

Figure 2. Marginalized posterior distribution for $\dot{n}_0$. The orange and green outlines show the posterior distributions for the M16 and C19 models, respectively. The filled green histogram shows the prior for C19 (the prior for M16 is uniform in the range $[-20, 3]$). The vertical dotted lines indicate the 5 per cent to 95 per cent central credible region.

4 RESULTS: IMPLICATIONS FOR THE MBHB POPULATION

Using the agnostic M16 model, the NANOGrav data mostly constrain the MBHB merger rate, described by the parameter $\log_{10}\dot{n}_0$; see Fig. 2. All other parameters return posterior distributions consistent

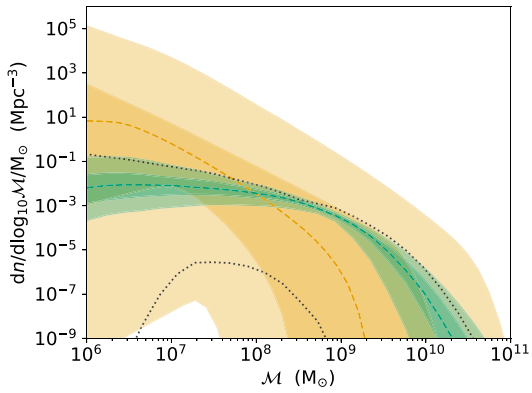

Figure 3. Merger rate density versus chirp mass posterior for the M16 and C19 analyses in orange and green, respectively. The shaded regions show the central 50 per cent and 90 per cent credible regions, and the dashed lines show the median. The black-dotted lines show the central 99 per cent region for the C19 prior.

with the priors (see Supplementary Material for full corner plots of both models). Constraining only a single parameter is unsurprising as we are using a single observational datum in the likelihood function, and the prior ranges cover many orders of magnitude in h_c. We find a central 90 per cent credible region (5 per cent to 95 per cent) from -10.9 to 0.3 in $\log_{10}\dot{n}_0$. In Fig. 2 we compare this to the equivalent effective parameter for the C19 model. The latter is constrained to a much narrower range by the astrophysical prior, and the posterior favours values on the high side of the allowed range. The posterior distribution peak is at $\log_{10}\dot{n}_0 \approx -4$, offset from the M16 model. Still, there is full consistency between the $\log_{10}\dot{n}_0$ posterior distributions for the two models, as the C19 posterior support is fully included within the M16 one.

The difference in the $\log_{10}\dot{n}_0$ is explained by the inference on the redshift-integrated MBHB mass function, as shown in Fig. 3. The astrophysical prior of C19 imposes a strict upper bound to the merging MBHB mass function across the mass range (upper black-dotted line). No such restriction is imposed in the M16 model, in which the low-mass end of the MBHB mass function – that does not contribute significantly to the amplitude of the SGWB – can be quite steep, resulting in a much higher integrated merger rate (i.e. higher $\log_{10}\dot{n}_0$).

Finally, we consider whether the NANOGrav measurement constrains any other interesting astrophysical parameter in the C19 model. Contrary to the M16 model, in C19 one does not start from a coalescing MBHB function, but from an astrophysically constrained population of galaxy pairs. Within these galaxies reside MBHs that might eventually merge following the galaxy merger. The formation and coalescence of the MBHBs are not postulated, but it is bound to a coalescence time-scale, which is described by a function of the form

$$\tau(M, z, q) = \tau_0 \left(\frac{M}{bM_0}\right)^{\alpha_\tau} (1+z)^{\beta_\tau} q^{\gamma_\tau}\,, \tag{7}$$

where τ_0 is an (unknown) constant which sets the overall time-scale, M is the primary galaxy mass, $q < 1$ is the galaxy mass ratio, and $bM_0 = 0.4/h_0 \times 10^{11}\mathrm{M}_\odot$. τ describes the typical time elapsed between two galaxies being at a (projected) distance of ≈ 30 kpc, where galaxy pairs are counted, and the final coalescence of the MBHB, including pairing via dynamical friction, hardening and final GW emission. Constraints on τ_0, α_τ, and β_τ are shown in Fig. 4. The data favour rapid coalescence of binary pairs, with characteristic

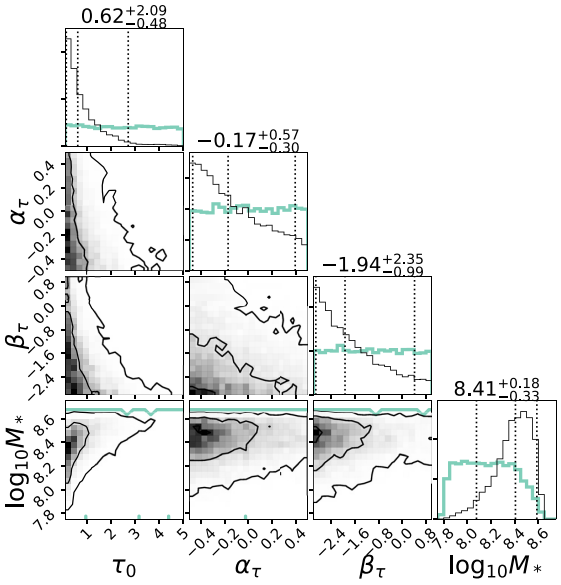

Figure 4. The 2D and 1D marginalized posterior distributions for selected parameters of the C19 model. Posteriors and priors are shown as black and green histograms, respectively.

$\tau_0 < 2.7$ Gyr (90 per cent confidence). The fact that both α_τ and β_τ posterior density functions are skewed towards negative values suggests short merger time-scales are preferred. For C19, the black hole mass $M_{\rm BH}$ is connected to the galaxy bulge mass $M_{\rm bulge}$ via a scaling relation of the form (see e.g. Kormendy & Ho 2013)

$$M_{\rm BH} = \mathcal{N}\left\{M_*\left(\frac{M_{\rm bulge}}{10^{11}\mathrm{M}_\odot}\right)^{\alpha_*}, \epsilon\right\}, \tag{8}$$

where $\mathcal{N}\{x, y\}$ is a lognormal distribution with mean x and standard deviation y. The measurement of a stochastic signal with $A_{\rm yr} \approx 2 \times 10^{-15}$ naturally favours high normalizations, $M_* \geq 1.2 \times 10^8\,\mathrm{M}_\odot$ (90 per cent confidence), resulting in a clear preference for high M_* (see the bottom-right panel of Fig. 4).

5 CONCLUSIONS

Our analysis of the astrophysical implications of the reported NANOGrav common stochastic red process (Arzoumanian et al. 2020), under the assumption that this signal is of astrophysical origin and due to an SGWB from a population of MBHBs, provides a consistent picture. Forward modelling of the SGWB signal from a comprehensive suite of Monte Carlo realisations of the MBHB population (Rosado et al. 2015) shows that the 2D credible region of the amplitude and spectral slope ($A_{\rm yr}$, γ) of the observed common red process is fully consistent with an SGWB produced by the incoherent superposition of radiation from MBHBs that are individually unresolvable. It also shows that $M_{\rm BH}$–$M_{\rm bulge}$ relations with high normalizations better reproduce the NANOGrav signal. Bayesian inference on a parametric agnostic model of the MBHB population (Middleton et al. 2016) shows that, without any other prior information, the detected signal implies an MBHB merger rate density in the range of 10^{-11}–$2\,\mathrm{Mpc}^{-3}\,\mathrm{Gyr}^{-1}$ (90 per cent credible interval), consistent with expectations from independent estimates of galaxy and MBHB merger models. Finally, using an observation-based parametric model (Chen et al. 2019), which introduces additional independent prior limits, we find that the NANOGrav results further constrain the MBHB merger rate to 1.2×10^{-5}–$4.5 \times 10^{-4}\,\mathrm{Mpc}^{-3}\,\mathrm{Gyr}^{-1}$. This

naturally favours high normalizations in the $M_{\rm BH}$–$M_{\rm bulge}$ relation, consistent with recent estimates in the literature (e.g. Kormendy & Ho 2013; McConnell & Ma 2013), and relatively short merger time-scales. All other parameters have posterior density functions consistent with the priors (see the Supplementary Material).

The common stochastic red process reported by NANOGrav is therefore fully consistent with our current knowledge of the cosmic MBHB population, although it is also consistent with a steeper red spectrum centred around $h_{\rm c} \propto f^{-1} - f^{-1.5}$, which has prompted a number of early Universe interpretations. In light of our findings, however, if future PTA analyses on longer and more sensitive data sets, and including a larger number of pulsars, provided stronger statistical significance for the detection of this signal, the MBHB scenario would offer a natural explanation without the need of invoking more exotic physical processes. Most importantly, the signal would provide direct evidence that MBHB mergers occur in nature. As timing campaigns from PTA groups around the world continue to provide more and higher sensitivity data, the next few years will be decisive (Pol et al. 2020) in assessing the statistical significance of current observational results, and shed light on the underlying astrophysical processes.

ACKNOWLEDGEMENTS

Parts of work were performed on the OzSTAR national facility at Swinburne University of Technology. The OzSTAR program receives funding in part from the Astronomy National Collaborative Research Infrastructure Strategy (NSCRIS) allocation provided by the Australian Government. HM is supported by the Australian Research Council Centre of Excellence for Gravitational Wave Discovery (OzGrav) (project no. CE170100004). AS is supported by the European Research Council (ERC) under the European Union's Horizon 2020 research and innovation program ERC-2018-COG under grant agreement no. 818691 (B Massive). SC acknowledges support from the CNRS, CEA, CNES in France. AV acknowledges support from the Royal Society and the Wolfson Foundation. The authors acknowledge support from the European Pulsar Timing Array (EPTA), the North American Nanohertz Observatory for Gravitational Waves (NANOGrav), the Parkes Pulsar Timng Array (PPTA), and the International Pulsar Timing Array (IPTA).

DATA AVAILABILITY

The posterior samples used to produce this work are available from https://github.com/hannahm8/PTAInference.

REFERENCES

Arzoumanian Z. et al., 2018, ApJ, 859, 47
Arzoumanian Z., et al., 2020, ApJL, 905, L34
Begelman M. C., Blandford R. D., Rees M. J., 1980, Nature, 287, 307
Chen S., Middleton H., Sesana A., Del Pozzo W., Vecchio A., 2017a, MNRAS, 468, 404
Chen S., Sesana A., Del Pozzo W., 2017b, MNRAS, 470, 1738
Chen S., Sesana A., Conselice C. J., 2019, MNRAS, 488, 401
Cornish N. J., Sesana A., 2013, Class. Quantum Gravity, 30, 224005
Detweiler S., 1979, ApJ, 234, 1100
Ellis J., van Haasteren R., 2017, jellis18/PTMCMCSampler,
Foster R. S., Backer D. C., 1990, ApJ, 361, 300
Graham A. W., 2012, ApJ, 746, 113
Hazboun J. S., Simon J., Siemens X., Romano J. D., 2020, ApJL, 905, L6
Hellings R. W., Downs G. S., 1983, ApJ, 265, L39
Kormendy J., Ho L. C., 2013, ARA&A, 51, 511
Lentati L. et al., 2015, MNRAS, 453, 2576
McConnell N. J., Ma C.-P., 2013, ApJ, 764, 184
Middleton H., Del Pozzo W., Farr W. M., Sesana A., Vecchio A., 2016, MNRAS, 455, L72
Middleton H., Chen S., Del Pozzo W., Sesana A., Vecchio A., 2018, Nat. Commun., 9, 573
Phinney E. S., 2001, preprint (arXiv astro–ph/0108028)
Pol N. S. et al., 2020, preprint (arXiv:2010.11950)
Rosado P. A., Sesana A., Gair J., 2015, MNRAS, 451, 2417
Sazhin M. V., 1978, Sov. Astron., 22, 36
Schechter P., 1976, ApJ, 203, 297
Sesana A., Vecchio A., Colacino C. N., 2008, MNRAS, 390, 192
Sesana A., Vecchio A., Volonteri M., 2009, MNRAS, 394, 2255
Shannon R. M. et al., 2015, Science, 349, 1522
Taylor S. R., van Haasteren R., Sesana A., 2020, Phys. Rev. D, 102, 084039
Veitch J., et al., 2021, johnveitch/cpnest
Veitch J., Vecchio A., 2010, Phys. Rev. D, 81, 062003
Verbiest J. P. W. et al., 2016, MNRAS, 458, 1267
White S. D. M., Rees M. J., 1978, MNRAS, 183, 341

SUPPORTING INFORMATION

Supplementary data are available at *MNRASL* online.

Figure S1 Marginalized posterior distributions for the five parameter M16 model.

Figure S2 Same as Fig. S1 but for the 18 parameters defining the C19 model.

Please note: Oxford University Press is not responsible for the content or functionality of any supporting materials supplied by the authors. Any queries (other than missing material) should be directed to the corresponding author for the article.

This paper has been typeset from a TEX/LATEX file prepared by the author.